Earth, Planets and Space

TECHNICAL REPORT

Open Access

CrossMark

Space environment data acquisition monitor onboard Himawari-8 for space environment monitoring on the Japanese meridian of geostationary orbit

Tsutomu Nagatsuma[1*], Kaori Sakaguchi[1], Yûki Kubo[1], Piet Belgraver[2], Frédéric Chastellain[2], Reto Muff[2] and Takeshi Otomo[3]

Abstract

A space environment data acquisition monitor (SEDA) has been flown onboard the Japanese meteorological satellites 'Himawari-8/9' as one of the housekeeping information monitors for satellite operation. SEDA consists of a high-energy proton sensor (SEDA-p) and a high-energy electron sensor (SEDA-e). These instruments provide near-real-time information on the conditions of the space environment on the Japanese meridian. Initial cross-comparison between SEDA and high-energy particle observation by geostationary operational environmental satellite (GOES) shows that the flux level of SEDA-e is slightly smaller than that of GOES observation, and the flux level of SEDA-p observation is a half that of GOES observation.

Keywords: Space weather, High-energy electron, High-energy proton, Geostationary orbit, Cross-comparison, Space environment monitoring

Background

The geostationary earth orbit (GEO) is one of the practical orbits of satellites providing our social infrastructure. More than 400 telecommunications, broadcasting, and meteorological satellites are currently operated in this orbit (e.g., http://www.satsig.net/sslist.htm Note: Military satellites in GEO are not included in this list). GEO is located at the outer edge of the outer radiation belt. Relativistic electrons in the outer radiation belt undergo dynamic changes because of the magnetospheric disturbances driven by solar wind. In addition, GEO satellites frequently experience the injection of energetic particles related to substorm activities. Variations in the charged particle environment are one of the causes of satellite anomalies (e.g., Lanzerotti et al. 1998; Baker 2000). For

these reasons, the monitoring and forecasting of the space environment in GEO is one of the key issues of space weather research and operation.

The monitoring of the high-energy particle environment in the Japanese meridian of GEO started at the beginning of Japan Meteorological Agency (JMA)'s satellite program. Space environment monitors (SEM) onboard Japan's geostationary meteorological satellite (GMS) series 'Himawari' have been started with GMS-1 in 1978 (Kurino 1985). Space environment monitoring by SEM continued up to GMS-4. However, SEM was not installed onboard the satellites that followed GMS-4 (GMS-5, MTSAT-1R, MTSAT-2). Thus, there was a large gap in space environment monitoring in the Japanese meridian of GEO from the mid-1990s to the mid-2010s.

The situation changed because a space environment data acquisition monitor (SEDA) was installed in Himawari-8/9 (Bessho et al. 2016). This action has also contributed to the World Meteorological Organization (WMO)'s recommendation of installing a space environment monitor in all meteorological satellites for housekeeping

*Correspondence: tnagatsu@nict.go.jp

[1] Space Environment Laboratory, Applied Electromagnetic Research Institute, National Institute of Information and Communications Technology, 4-2-1 Nukui-kita, Koganei, Tokyo 184-8795, Japan

Full list of author information is available at the end of the article

Nagatsuma *et al. Earth, Planets and Space* (2017) 69:75

Page 2 of 8

information and space environment monitoring (e.g., WMO 2013). Himawari-8 and 9 were launched on October 7, 2014, and November 2, 2016, respectively. SEDA onboard Himawari-8 and 9 has been in operation since November 3, 2014, and December 20, 2016, respectively.

The National Institute of Information and Communications Technology (NICT) has a long history of operational space weather forecasting in Japan (Nagatsuma 2013). Space environment monitoring is one of the key elements in space weather forecasting. Since 1979, we have received a daily summary plot of SEM from JMA, and a real-time data acquisition system for GMS-4/SEM has been in operation since 1994 (Den et al. 1999). On the basis of this background, we are now handling and processing Himawari-8/SEDA data for space environment monitoring in the Japanese meridian of GEO. In this paper, we briefly introduce the instrumentation of SEDA, the initial observations, and the results of our initial cross-comparison with geostationary operational environmental satellite (GOES) data.

Instrumentation

SEDA has been flown onboard Himawari-8 and 9 to monitor the space environment around the satellite. The basic specifications of SEDA are shown in Table 1. Figure 1 shows the fully assembled SEDA. This sensor is identical to the Environmental Monitor Unit (EMU) for the European Galileo satellite series (Bartolomé et al. 2015). SEDA consists of two sensors, namely a high-energy proton sensor (SEDA-p) and a high-energy electron sensor (SEDA-e). SEDA-p and SEDA-e have eight channels each, the energies of which are shown in Table 2. The large cylinder on the right side of the SEDA assembly in Fig. 1 is SEDA-e, whereas SEDA-p comprises the eight small cylinders on the left side in Fig. 1. The intermediate-size cylinder on the left side has no use.

SEDA obtains data every 10 s based on the clock in the SEDA assembly. Because of the time difference between the clock in the main satellite system and that in SEDA, the measurement timing drifts by about one second per day. The sampling rate sometimes shifts by 9 or 11 s owing to the jitter of the clock in SEDA.

SEDA is mounted on the eastward plane on the body of Himawari-8 and 9. Owing to the gyro motion of charged particles, SEDA can measure protons whose gyro centers lie inside GEO and electrons whose gyro centers lie outside GEO (Rodriguez et al. 2010). The geographical longitude and local noon of Himawari-8 and 9 are 140.7° and 02:37 UT, respectively.

Real-time data observed by Himawari/SEDA are downlinked to JMA's Meteorological Satellite Center, where they are routinely stored on file servers. Every 10 min, we download the latest files of Himawari/SEDA data from

Table 1 Specifications of SEDA

Items	Description
Number of channels	Protons: 8 (8 individual sensor elements)
	Electrons: 8 (8 stacked plates in one element)
Energy range	Protons: 15–100 MeV
	Electrons: 0.2–4.5 MeV
Time resolution	10 s
Field of view	Protons: ±39.35°
	Electrons: ±78.3°

Fig. 1 Fully assembled SEDA

the server to monitor the space environment at the Japanese meridian of GEO.

SEDA high-energy electron sensor (SEDA-e)

SEDA-e is not a direct-particle-counting-type sensor but a sensor for measuring the internal charging current deposited by the energetic electron flux at various shielding levels. Because the penetrating energy of electrons depends on the material thickness, the electrons which have a specific range of energy can be accumulated using a shield and a collector plate. SEDA-e consists of eight metal plates mounted on a stack for measuring eight different energy ranges from 0.2 to 4.5 MeV. There is no additional shielding between each collector plate.

The SEDA-e sensor is based on the SURF sensor and is also used as an internal charging current monitor. The SURF sensor was first demonstrated in space by the Space Technology Research Vehicle (STRV) 1D in geostationary transfer orbit in 2000 (Ryden et al. 2001). Furthermore, the SURF sensor was installed as part of the Merlin space weather monitors onboard GIOVE A, a test bed for Galileo launched in 2005. The SURF sensor has completed 8.5 years in orbit despite being originally intended to have a two-year operational life (Ryden et al. 2015). One of the advantages of this sensor is its robustness against high-energy proton contamination compared with a semiconductor-type sensor. Because of the weak current deposited from the high-energy electron

Nagatsuma *et al. Earth, Planets and Space* (2017) 69:75

Page 3 of 8

Table 2 Energies of proton and electron channels

Ch. no.	Proton energy (MeV)	Electron energy (MeV)
0	21.6	0.2
1	29.9	0.3
2	37.9	0.45
3	45.4	0.65
4	57.8	1.0
5	68.4	1.5
6	75.2	2.0
7	81.4	4.5

flux, the signals are amplified by an electrometer with an input bias current, which is dependent on the sensor's temperature. To estimate the flux of energetic electrons, the effect of the bias current is removed using empirical equations with temperature information of the sensor.

SEDA high-energy proton sensor (SEDA-p)

SEDA-p measures the proton flux in eight energy channels from 15 to 100 MeV via individual telescopes. Each telescope has a detector diode on the top and bottom. All energy deposition events above a certain threshold (i.e., non-coincident detection) are counted by the top detector. The coincidences for particles arriving within the detector opening angle are selected by the bottom detector. A proton that is detected simultaneously by both the top and bottom detectors is counted as coincident.

Observation of high-energy particle environment by SEDA

Figures 2 and 3 show examples of high-energy particle observations by Himawari-8/SEDA on March 15–20, 2015, and October 27–31, 2015, respectively. The 5-min running mean of SEDA-e electron differential fluxes and SEDA-p proton differential fluxes in the eight channels and the provisional Dst index are plotted from the top to bottom panels in these figures.

Figure 2 shows that a strong geomagnetic storm occurred from March 17 to 20. The minimum Dst is −223 nT at 23 UT on March 17. The daily variations of the electron fluxes from Channels (Chs.) 0–5 have a peak at around 02–03 UT, which is near the local noon of Himawari-8. This signature is consistent with previous high-energy particle observations by other GEO satellites. In contrast, the electron fluxes of Chs. 6 and 7 have different phases of daily variations, which have a peak at around 14–15 UT. However, on March 19 and 20, the electron flux variations of Ch. 6 tend to correspond to those of the lower channels. Short-term variations that are related to substorm activities during the storm, and flux enhancement after the storm can be clearly seen.
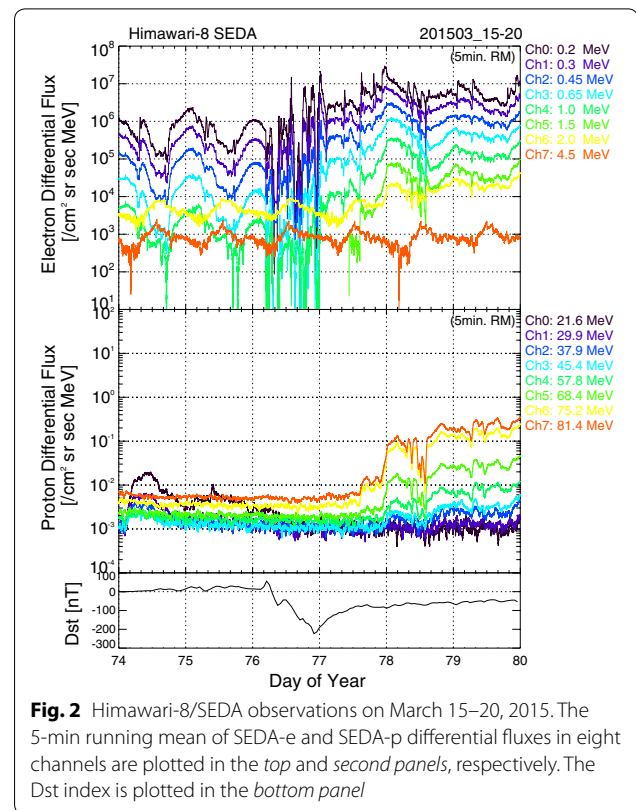

Fig. 2 Himawari-8/SEDA observations on March 15–20, 2015. The 5-min running mean of SEDA-e and SEDA-p differential fluxes in eight channels are plotted in the *top* and *second panels*, respectively. The Dst index is plotted in the *bottom panel*
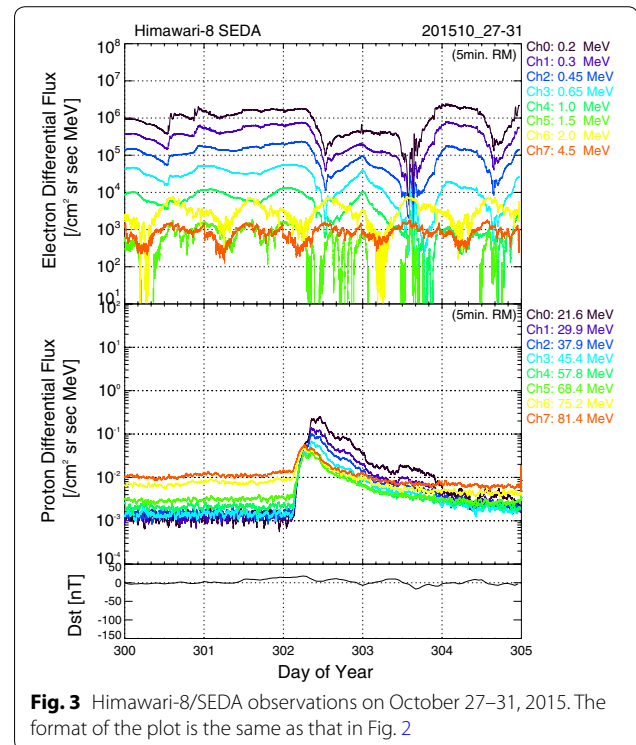

Fig. 3 Himawari-8/SEDA observations on October 27–31, 2015. The format of the plot is the same as that in Fig. 2

Nagatsuma *et al. Earth, Planets and Space* (2017) 69:75

Page 4 of 8

Weak flux enhancements of high-energy protons are observed in Ch. 0 from March 15 to 17 and in Chs. 1–3 on Mar. 15. The proton fluxes from Chs. 4–7 show no significant variations from March 15 to 17. An apparent enhancement of the proton flux from Chs. 2 to 7 is also observed from March 18 to 20. One of the surprising characteristics of this enhancement is that there appears to be spectral inversion, with the higher channels showing larger flux as well as possibly larger flux variations. The trend of this enhancement is almost coherent for each channel and appears to be related to the variations of high-energy electron fluxes. The relationship between Ch. 7 of SEDA-p and Ch. 6 of SEDA-e is shown in Fig. 4. The flux enhancement of SEDA-p Ch. 7 corresponds well to that of SEDA-e Ch. 6.

An example of a minor proton event that occurred on October 29, 2015, is shown in Fig. 3. The higher proton channels show higher flux levels on October 27 and 28. In this event, the proton flux shows a two-step enhancement. Time profile of proton flux variations can be distinguished in two groups. The first rapid enhancement of the proton flux from Chs. 0–7 occurred at around 03:10 UT with energy dispersion. Higher-energy channels tend to show earlier enhancement. The second enhancement of the proton flux from Chs. 0–4 occurred at around 07:10 UT. The proton flux of the lower-energy channels shows a significant increase during the second enhancement. However, the second enhancement shows no clear energy dispersion. The reason of the different time profile of these two enhancements is not clear. It might be caused by the characteristic of response function for each channels or natural phenomena. The electron flux variation

does not show any correspondence with the proton flux variation during this minor proton event.

Quality check of SEDA data

To examine the quality of SEDA data, it is important to compare the data with high-energy particle data observed by other GEO satellites. The differences in the *L*-value among the GEO satellites need to be taken into account for the cross-comparison of particle data, because the magnetic dipole axis is not aligned with the rotational axis of Earth. The *L*-value of each GEO satellite also changes with geomagnetic disturbances and depends on the local time. Figure 5 shows Roederer's *L* (*L**)-value of GEO estimated from the Tsyganenko 89 (T89) model under quiet conditions at 00 UT on Jan. 01, 2015 (Tsyganenko 1989), where *L** is the magnetic drift invariant proposed by Roederer (1970). In Fig. 5, the *L**-values of Himawari-8, GOES 15, and GOES 13 are 6.03, 5.94, and 6.39, respectively. This suggests that the drift shell of GOES 15 is close to that of Himawari-8. We use high-energy particle data obtained from the Magnetospheric Electron Detector (MAGED) (Hanser 2011) and the Energetic Proton, Electron and Alpha Detector (EPEAD) (Onsager et al. 1996; Hanser 2011) onboard GOES 15 in our data analysis. The energy channels of MAGED and EPEAD are shown in Tables 3 and 4, respectively. Note that the high-energy electron channels of EPEAD measure the integral flux, whereas SEDA-e measures the differential flux of high-energy electrons.

Estimating differential flux from observed integral fluxes

Because EPEAD measures the integral flux of high-energy electrons, we need to estimate the differential flux from
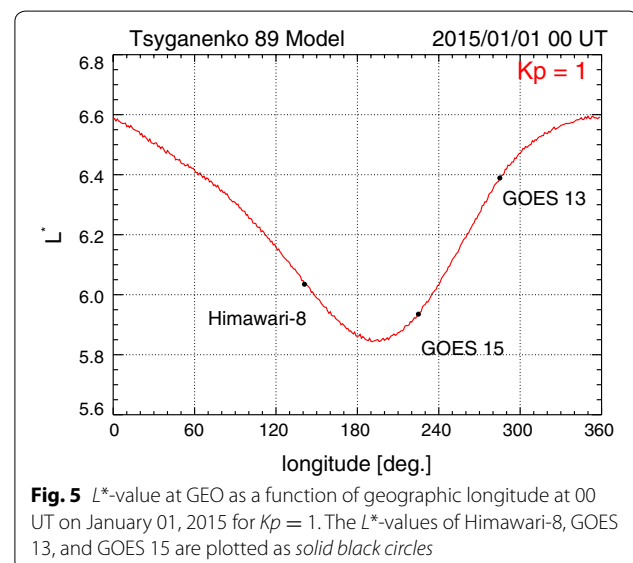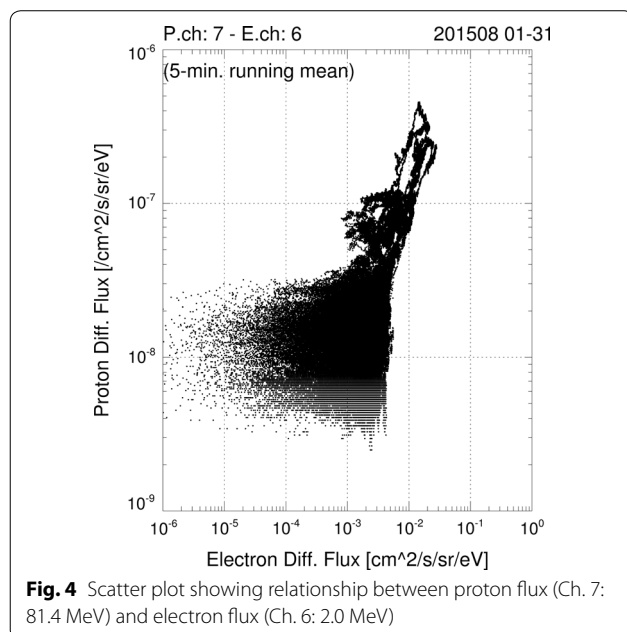

Fig. 4 Scatter plot showing relationship between proton flux (Ch. 7: 81.4 MeV) and electron flux (Ch. 6: 2.0 MeV)

Fig. 5 *L**-value at GEO as a function of geographic longitude at 00 UT on January 01, 2015 for *Kp* = 1. The *L**-values of Himawari-8, GOES 13, and GOES 15 are plotted as *solid black circles*

Nagatsuma *et al. Earth, Planets and Space* (2017) 69:75

Page 5 of 8

Table 3 Energy range of GOES MAGED

Ch. no.	Energy range (keV)
1	30–50 (40)
2	50–100 (75)
3	100–200 (150)
4	200–350 (275)
5	350–500 (475)

Table 4 Energy range of GOES EPEAD

Ch. no	Proton energy (MeV)	Electron energy (MeV)
1	0.7–4	>0.8
2	4–9	>2.0
3	9–15	>4.0
4	15–40	
5	38–82	
6	84–200	
7	110–900	

integral fluxes. Onsager et al. (2004) introduced a method of estimating the phase space density with a 90° pitch angle at the magnetic equator by assuming the exponential distribution of the phase space density and the pitch angle distribution at the equator using two channels for integral flux observation by EPEAD. We adopt the method of Onsager et al. (2004) for our data analysis. In his method, the distribution of the phase space density is expressed as the following exponential equation:

$$f(E) = f_0 \exp\left(-E/E_0\right). \quad (1)$$

Equation (1) can effectively represent the energetic electron spectra observed at GEO (e.g., Cayton et al. 1989). On the basis of this assumption, the relationship between the phase space density $f(E)$ and the observed integral flux $J(>E)$ is written as

$$f(E) = c^2 J(> E)/\left(\left(E_0^2 + EE_0\right)2m_e c^2 \right. \\ \left. + 2E_0^3 + 2EE_0^2 + E^2 E_0\right), \quad (2)$$

where c is the speed of light and m_e is the rest mass of an electron.

Using the integral flux observed in two channels (>0.8 and >2.0 MeV) from EPEAD, we can estimate f_0 and E_0. The differential flux $j(E)$ is calculated from the following equation using the estimated f_0 and E_0:

$$j(E) = p^2 f(E) = \left((E/c)^2 + 2m_e c^2 E\right) f_0 \exp\left(-E/E_0\right), \quad (3)$$

where p is the particle momentum. Using this method, differential fluxes of 1.0, 1.5, and 2.0 MeV are estimated

from EPEAD onboard GOES 15. Gannon et al. (2012) already used the same technique to estimate differential flux from GOES EPEAD data.

Cross-comparison between Himawari-8/SEDA, GOES 15/MAGED, and GOES 15/EPEAD

Figure 6 shows scatter plots revealing the relationship between Himawari-8/SEDA-e and GOES 15/MAGED (left) and that between Himawari-8/SEDA-e and GOES 15/EPEAD (right). In this analysis, we only use one-hour-averaged flux at each noon local time data for comparison. Although the geographical locations of Himawari-8 and GOES 15 on GEO are almost opposite each other, the correlation between the two particle sensors shows reasonably good agreement. The flux level of SEDA-e is slightly smaller than that of GOES observation.

Figure 7 shows the combined energy spectra of electrons obtained from Himawari-8/SEDA, GOES 15/MAGED, and GOES 15/EPEAD on March 9, 2015. The energy spectra obtained from both satellites show good agreement during this period, although the flux level of Himawari-8/SEDA is slightly lower than that of GOES 15/EPEAD and MAGED.

Few proton events have occurred since the Himawari-8/SEDA started operation. Thus, the proton fluxes of SEDA and EPEAD cannot be statistically examined and compared. Figure 8 shows the combined plot of proton energy spectra from Himawari-8/SEDA (red) and GOES 13/EPEAD (black) at 10:45 UT on Oct. 29, 2015. Sandberg et al. (2014) have examined the effective energies of GOES solar proton detectors using corrected interplanetary monitoring platform (IMP) 8 solar proton measurements. As shown by Rodriguez et al. (2017), agreement is greatly improved between GOES and STEREO when using the effective energies estimated by Sandberg et al. (2014). So, we also apply this effective energy of EPEAD in our analysis. Green line with filled circles shows differential flux of GOES 13/EPEAD channels with effective energies derived from Sandberg et al. (2014). Although Sandberg et al. (2014) estimated effective energies of GOES 11/EPEAD, that information can be used as effective energies of GOES 13/EPEAD with reasonable accuracy based on the inter calibration study done by Rodriguez et al. (2014). To determine the energy spectra, 5-min-averaged data with the background flux level caused by galactic cosmic rays subtracted are used. The energy spectrum of SEDA-p shows a power law distribution, except for Chs. 6 (75.2 MeV) and 7 (81.4 MeV). The flux enhancement seen in Chs. 6 and 7 appears to show contamination with high-energy electron flux, since flux of high-energy proton and that of high-energy electron has some correlation shown in Fig. 4. The energy spectrum of EPEAD shows a power-law distribution with
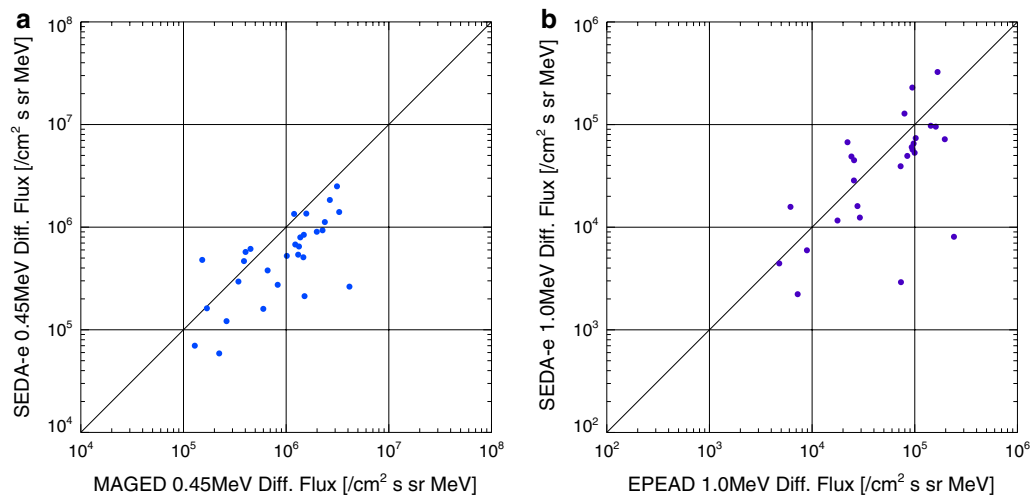
Nagatsuma *et al. Earth, Planets and Space* (2017) 69:75

Page 6 of 8

Fig. 6 a Scatter plot showing relationship between electron flux at 0.45 MeV estimated from SEDA-e and that estimated from MAGED. **b** Scatter plot showing relationship between electron flux at 1.0 MeV estimated from SEDA-e and that estimated from EPEAD
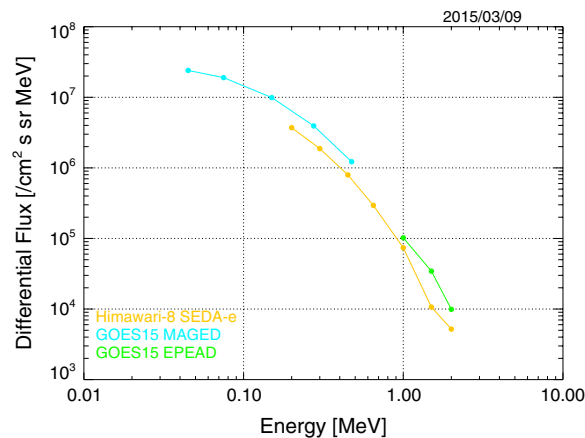

Fig. 7 Combined electron differential flux spectra from Himawari-8/SEDA (*orange*), GOES-15/MAGED (*light blue*), and GOES-15/EPEAD (*green*) on March 9, 2015
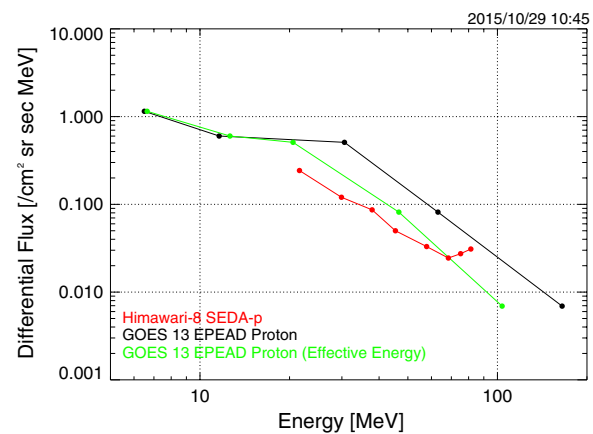

Fig. 8 Combined proton differential flux spectra from Himawari-8/SEDA (*red*), GOES-13/EPEAD (*black*) and GOES-13/EPEAD with effective energy (*green*) at 10:45 UT on Oct. 29, 2015

a bump at around 30 MeV. The proton flux of GOES 13/EPEAD with effective energy is about two times higher than that of Himawari-8/SEDA-p. However, the slope of the power law is almost the same for those energy spectra.

Summary and discussion

As we mentioned earlier, this instrument was originally developed as the EMU onboard the European Galileo satellite. The specifications of this instrument are optimized for observations on medium earth orbit, which is the orbit of Galileo. Thus, the sensitivity of the sensor is slightly low to cover the dynamic range of high-energy particle observations at GEO, especially for Chs. 6 and 7 of SEDA-e.

The trend of the daily variation seen in Chs. 6 and 7 of SEDA-e appears to be residuals of the bias current subtraction, because the daily variation of the temperature of SEDA is in phase (data not shown). The daily and long-term trends of the electron flux variations in Ch. 7 and their relation with the sensor temperature trend suggest that the effect of the bias current still remains. The subtraction of the bias current effect from the raw data of SEDA-e will be improved by detailed analysis of the relationship between the electron flux and the sensor temperature.

One of the advantages of SEDA-e is that high-energy proton flux contamination is negligible. Thus, high-energy electron flux variations during a proton event

Nagatsuma *et al. Earth, Planets and Space* (2017) 69:75

Page 7 of 8

can be captured by SEDA-e. In contrast, contamination by high-energy electron flux is apparent in most of the SEDA-p channels. It is well known that detector diode has a sensitivity of both high-energy electrons and protons [e.g., Fig. 2 of Takagi et al. (1993)]. However, SEDA-p cannot discriminate high-energy protons and electrons on board because of simple instrument for monitoring purposes. Removing the electron flux contamination based on data processing on the ground is not easy because the high-energy electron channels (Chs. 6 and 7) can only measure the high-flux period. Another future task is to improve the data quality of SEDA-p. Problems in the removal of electron contamination from proton flux data and the improvement of bias current subtraction from electron flux data will be solved in the near future.

The cross-comparisons between differential flux of Himawari-8/SEDA-e and that of GOES 15/MAGED in Fig. 6 show good correspondence. However, each data point also shows some degree of scattering. It seems that the time difference of each differential flux at noon local time produces the difference. So, we should select the period when Himawari-8 and GOES 15 are in the same L^* at the same time for cross-calibration.

Himawari-8/SEDA data are useful for monitoring the high-energy particle environment around the Japanese meridian of GEO. Near real-time plot and archived data of SEDA are available from our web site (http://seg-web.nict.go.jp/himawari-seda/). Furthermore, combining Himawari-8/SEDA data with other satellite data in GEO (e.g., GOES 13, 15, and Kodama (JAXA's Data Relay Test Satellite)) will enable us to estimate the particle distribution in the whole area of GEO. Developing a method for cross-calibration of the particle sensor will be one of the important tasks for reconstructing the particle distributions around GEO and the inner magnetosphere.

Abbreviations
SEDA: space environment data acquisition monitor; GEO: geostationary earth orbit; GOES: geostationary operational environmental satellite; JMA: Japan Meteorological Agency; SEM: space environment monitor; GMS: geostationary meteorological satellite; WMO: World Meteorological Organization; NICT: National Institute of Information and Communications Technology; EMU: environmental monitor unit; STRV: space technology research vehicle; MAGED: magnetospheric electron detector; EPEAD: energetic proton, electron and alpha detector; IMP: interplanetary monitoring platform.

Authors' contributions
TN performed the initial analysis of SEDA data and the cross-comparison between SEDA and other satellite data. KS carried out the quality check of the high-energy electron data. YK carried out the quality check of the high-energy proton data and discussed about the cause of contamination. PB, FC, and RM manufactured and tested the SEDA instrument. TO constructed the data acquisition system of Himawari-8/SEDA.

Author details
[1] Space Environment Laboratory, Applied Electromagnetic Research Institute, National Institute of Information and Communications Technology, 4-2-1 Nukui-kita, Koganei, Tokyo 184-8795, Japan. [2] Thales Alenia Space Switzerland Ltd, Zurich, Switzerland. [3] Satellite Program Division, Japan Meteorological Agency, 1-3-4 Otemachi, Chiyoda-ku, Tokyo 100-8122, Japan.

Competing interests
The authors declare that they have no competing interests.

Publisher's Note
Springer Nature remains neutral with regard to jurisdictional claims in published maps and institutional affiliations.

References
Baker DN (2000) The occurrence of operational anomalies in spacecraft and their relationship to space weather. IEEE Trans Plasma Sci 28:2007–2016

Bartolomé JP, Maufroid X, Hernández IF, Salcedo JAL, Granados GS (2015) Chapter 2 Overview of Galileo system. In: Nurmi J, Lohan ES, Sand S, Hurskainen H (eds) GALILEO positioning tehcnology, 3rd edn. Springer, Dordrecht. doi:10.1007/978-94-007-1830-2_2

Bessho K, Date K, Hayashi M, Ikeda A, Imai T, Inoue H, Kumagai Y, Miyakawa T, Murata H, Ohno T, Okuyama A, Oyama R, Sasaki Y, Shimazu Y, Shimoji K, Sumida Y, Suzuki M, Taniguchi H, Tsuchiyama H, Uesawa D, Yokota H, Yoshida R (2016) An introduction to Himawari-8/9 - Japan's new-generation geostationary meteorological satellites. J Meteorol Soc Jpn. doi:10.2151/jmsj.2016-009

Cayton TE, Belian RD, Gary SP, Fritz TA, Baker DN (1989) Energetic electron components at geosynchronous orbit. Geophys Res Lett 16:147–150. doi:10.1029/GL016i002p00147

Den M, Obara T, Tomita F (1999) Development of GMS data acquisition and database systems. Adv Polar Upper Atmos Res 13:191–196

Gannon JL, Elkington SR, Onsager TG (2012) Uncovering the nonadiabatic response of geosynchronous electrons to geomagnetic disturbance. J Geophys Res 117:A10215. doi:10.1029/2012JA017543

Hanser FA (2011) EPS/HEPAD calibration and data handbook, Tech. Rep. GOESN-ENG-048D, Assurance Technol. Corp., Carlisle, Massachusetts

Implementation Plan for the Evolution of Global Observing Systems (EGOS-IP), WMO Integrated Global Observing System, Technical Report No. 2013-4

Kurino T (1985) Report on the utilization of space environment monitor (SEM) data of the GMS series satellite (in Japanese), Meteorological Satellite Center Technical Note, 12:45–55

Lanzerotti LJ, Breglia C, Maurer DW, Johnson GK III, Maclennan CG (1998) Studies of spacecraft charging on a geosynchronous telecommunications satellite. Adv Space Res 22:79–82. doi:10.1016/S0273-1177(97)01104-6

Nagatsuma T (2013) New ages of operational space weather forecast in Japan. Space Weather. doi:10.1002/swe.20050

Onsager TG, Grubb R, Kunches J, Matheson L, Speich D, Zwickl R, Sauer H (1996) Operational uses of the GOES energetic particle detectors. In: Proceedings of SPIE 2812, GOES-8 and Beyond, 281 (October 18, 1996). doi:10.1117/12.254075

Nagatsuma *et al. Earth, Planets and Space* (2017) 69:75

Page 8 of 8

Onsager TG, Chan AA, Fei Y, Elkington SR, Green JC, Singer HJ (2004) The radial gradient of relativistic electrons at geosynchronous orbit. J Geophys Res 109:A05221. doi:10.1029/2003JA010368

Rodriguez JV, Onsager TG, Mazur JE (2010) The east-west effect in solar proton flux measurements in geostationary orbit: a new GOES capability. Geophys Res Lett 37:L07109. doi:10.1029/2010GL042531

Rodriguez JV, Krosschell JC, Green JC (2014) Intercalibration of GOES 8–15 solar proton detectors. Space Weather 12:92–109. doi:10.1022/2013SW000996

Rodriguez JV, Sandberg I, Mewaldt RA, Daglis IA, Jiggens P (2017) Validation of the effect of cross-calibrated GOES solar proton effective energies on derived integral fluxes by comparison with STEREO observations. Space Weather 15:290–309. doi:10.1002/2016SW001533

Roederer JG (1970) Dynamic of geomagnetically trapped radiation, physics and chemistry in space, vol 2. Springer, Berlin

Ryden KA, Rodgers DJ, Morris PA, Frydland AD, Jolly HS, Dyer CS (2001) Direct measurement of internal charging currents in geostationary transfer orbit. In: Proceedings of the 6th RADECS conference, pp 44–50

Ryden KA, Hands ADP, Underwood CI, Rodgers DJ (2015) Internal charging measurements in medium Earth orbit using the SURF sensor: 2005–2014. IEEE Trans Plasma Sci 43:3014–3020

Sandberg I, Jiggens P, Heynderickx D, Daglis IA (2014) Cross calibration of NOAA GOES solar proton detectors using corrected NASA IMP-8/GME data. Geophys Res Lett 41:4435–4441. doi:10.1002/2014GL060469

Takagi S, Nakamura T, Kohno T, Shiono N, Makino F (1993) Observation of space radiation environment with EXOS-D. IEEE Trans Nucl Sci NS-40:1491–1497. doi:10.1109/23.273513

Tsyganenko NA (1989) A magnetospheric magnetic field model with a warped tail current sheet. Planet Space Sci 37:5–20